Waste heat recovery, utilization and evaluation of coalfield fire applying heat pipe associated thermoelectric generator in Xinjiang, China

Jinchang Deng [c], Fubao Zhou [a,b,c,*], Bobo Shi [a,b,c,*], Haining Qi [c], Peng Liu [c], José L. Torero [d], Zhiyu Wang [c], Shaokun Ge [c], Chen Chen [c].

[a] *Jiangsu Key Laboratory of Fire Safety in Urban Underground Space, China University of Mining and Technology, Xuzhou, 221116, China;* [b] *Key Laboratory of Gas and Fire Control for Coal Mines, China University of Mining and Technology, Ministry of Education, Xuzhou, 221116, China;* [c] *School of Safety Engineering, China University of Mining and Technology, Xuzhou, 221116, China;* [d] *UCL, Dept Civil Environmental & Geomatic Engineering, London, UK.*

Abstract: Coalfield subsurface fires can result in ecological disasters of global dimensions. These fires are difficult to control therefore can result in colossal wastage of resources (the coal itself but the resources devoted to suppression), a serious negative impact on the environment and acute health problems for large populations. However, if the heat can be effectively recycled and utilized, the combustion energy will be recovered but also heat extraction can promote suppression. Thus, leading not only to a positive energy impact but to a reduction polluting emissions and consequent health issues. This paper presents the results of a feasibility analysis of the overall recovery of underground thermal resources of a novel system of Waste Heat Recovery Units (WHRUS) that combines thermosyphon and thermoelectric technologies. Both thermal equivalent model and numerical assessment are presented. A series of realistic-scale field experiment conducted in the Xinjiang's fire zone for an extended period are discussed. Using a local geothermic assessment, the heat recovered from subsurface coal fire can be estimated as the summation of the convective and conductive components of the energy generated. The average heat generated for the fire district is estimated at approximately 495 W/m^2 and the average extraction efficiency at approximately 58%. The WHRUS shows and excellent heat transfer performance with an effective lower resistance of approximately 0.0049 W/°C and maximum thermal recovery rate greater than 90%. Finally, while the thermoelectric

[*] Corresponding authors

Tel: +86-516-83995053; Fax： +86-516-83995053

E-mail: f.zhou@cumt.edu.cn (F. Zhou); shi_bobo@yeah.net (B. Shi)

conversion efficiency is low, the power generated remains stable and on average every wellbore produces more than 960 W. The majority of the extracted heat is used to heat water for regional heating delivering an approximate efficiency of 38%. Through this process approximately 105 MW/a of otherwise wasted heat could be recovered from the entire investigated fire zone.

Keywords: Coal fire; waste heat recovery; utilization; heat pipe; thermoelectric generator; thermal evaluation.

Nomenclature	
A	area, m^2
A_0	unribbed side area, m^2
A_1	smoke radiation area, m^2
A_2	drivepipe radiation area, m^2
C	gray body emissivity, m^2·K^4
C_p	specific heat capacity, J/kg·°C
E	thermal electromotive force, V
L	length, m
$\bar{L}$	characteristic length of HP, m
H	vertical depth of the formation, m
h_{fg}	heat of vaporization, J/kg
I	currency, A
P	pressure, Pa
P_{TEG}	power of TEG, W
Q	heat transfer rate, W
q_{wt}	water flow, m^3/h
q	heat flow (flux), W/m^2
q'	air convection heat flow, W/m^2
R	thermal resistance (K/W)
R_g	gas constant (J/kg·K)
r_{TEG}	electric resistance of TEG, Ω
r_{max}	maximum electric resistance, Ω
r	radius, m
S_e	Seebeck coefficient, V/K
T	temperature, °C
T_h (T_c)	hot (cold) end temperature of TEG, °C
U	voltage, V
Z	the factor of merit of the TE materials, 1/K
ZT	the dimensionless figure of merit
Greek symbols	
α	convention coefficient, W/(m^2·°C)
α_c	convention of laminar film condensation, W/(m^2·°C)
α_e	convention of nucleate boiling, W/(m^2·°C)
β	contact rate of drivepipe, 0.01
η	efficiency, %
ρ	density, kg/m^3
v	dynamic viscosity, Pa·s
μ	mathematical expectation
σ	mean square deviation
K	electrical resistivity, Ω·m
λ	thermal conductivity, W/m·°C
Subscripts	
Al	Aluminum
ave	average
c (cond)	condenser section
conv	convection
comm	commom
CS	cold source
dp	drivepipe
e (evap)	evaporator section
f	film
HP	heat pipe
HS	heat source
i	inner
ih	indoor heating
m	measure
o	outer
radi	radiation
ra	radiator
sm	smoke
v	vapor
w	wall
wt	water

1. Introduction and background

Subsurface coal fires are a geological disasters that occurs in underground coal seams that are usually spontaneously ignited [1]. A series of complex reactions can take place when coal is in contacts with oxygen under favorable conditions leading to the gradual development of an intense combustion reaction. These are high temperature reactions that can occur within a very large volume for a long period of time. In consequence, the environmental impact is exceptionally serious [2]. According to reports, coal fire catastrophes have mainly occurred in China, the USA, Australia, Russia, India, Poland and South Africa, nevertheless, this seems to be a global problem [3-5]. The impact of coalfield fires on the environment and human health can therefore not be ignored [6]. Notably, large amounts of greenhouse gases (CO_2 and CH_4) [7-9], toxic gases (CO, SO_2, H_2S, N_2O, NO_x, etc.) and trace elements (As, F, Se, Hg, etc.) released by coal fires have significant global warming potential but also bring about problems such as smog, acid rain and toxic pollutions[10-13]. Vegetation is also destroyed by the heat exacerbating acidification and desertification of land [7]. Finally, coal fires, as they consume the coal, lead to surface subsidence and collapse.

China is globally the largest coal producer but also the country with the most subsurface coal fires. About 20 million tons of coal is consumed by serious coal fires every year [3, 5]. Thus, this problem is of particular importance for China.

The coal fires release massive amounts of energy that is trapped and accumulates in the rocks and stratum, which is similar to shallow geothermal energy reservoirs [18]. Given that typical field temperatures are between 300 and 400 °C, subsurface coal fires can be classified as the low-medium grade geothermal energy sources [19]. However, during suppression procedures, the heat is usually dissipated to the atmosphere by water cooling rather than reused [20]. Multiple studies have described these procedures and advanced techniques of fire detection and fire-extinguishing have been developed and reported over the past decades [5, 14-16]. In contrast, coal-fire energy recovery has received lesser attention with almost no literature available.

Energy recovery from subsurface coal fires is a complex problem that requires understanding of geological details, complex transport and combustion processes and spatial and temporal environmental impact that remains intractable and unmanageable by conventional methods. Thus, subsurface fires remain extremely harmful, unpredictable, persistent, and costly.

Recently, HP based systems have been extensively utilized in heat recovery. Examples are, industrial heat production [23], energy storage [24], geothermal energy [25], automotive engine [26] and solar energy [27]. In oil engineering, the ultra-long gravity HP transfers heat from the deeper oil production boreholes so that the geothermal energy can be recovered so it can then be used by the support utilities [30]. In a similar manner, several studies have described geothermal recovery in abandoned coal mines [31, 32]. An HP exchanger system was implemented to recycle the waste heat in mines for heating and air-conditioning [33].

Recovered heat needs to be effectively converted into useful forms of energy, this represents its own challenges in the context of a sub-surface coal fire. Thermoelectric generator (TEG) represent a good candidate technology for this specific application. TEG's have received significant attention recently, in particular for applications associated to electronics [34], buildings and vehicles[35, 36], and industrial systems [37-40]. The merits of TEG include the absence of airborne emissions and noise pollution, fabrication simplicity, flexibility, low maintenance and long life-span [41]. Nevertheless, the conversion efficiency of TEG still remains low and the cost of the Thermo-Electric devices (TE) is still high [42], despite recent breakthroughs in the development of these technologies [43]. Thus TEG is generally only viable when the source of heat is very large and cheap, making the cost of the device and efficiency less important. Sub-surface coal fires meet both requirements, thus TEG are an ideal candidate for energy recovery.

Most research in the application of TEG to sub-surface fires has been laboratory based or theoretical [45], with very limited information being reported at realistic scales. Recently, a HP exchanger system was tested for TEG in a sub-surface coal fire [17, 44]. The authors report that the maximum installed capacity was of 1600 W when using Bi_2Te_3 thermoelectric modules. While demonstrating that these systems can be used for this specific application, the specific arrangements proved to be inefficient and unstable delivering an unreliable source of power.

From a suppression perspective, the use of an HP is an effective way to take energy away from the reaction front promoting quenching of the smoldering reaction. HP has been used to enhance heat dissipation and impede heat accumulation in laboratory experiments as well as field demonstrations [28, 29]. In both settings, the HP reduced the temperature and eliminated the internal accumulation of energy.

The approach described in this paper requires the application of a Closed Loop Two Phase Thermosyphon (CLTPT) system. This is a wickless, gravity-assisted heat pipe (HP) device that transfers heat efficiently over a long distance only needing a small temperature differential and without any additional energy contribution [21]. This system relies on super thermal conductivity to deliver high unidirectional heat transfer efficiency and rapid temperature uniformity [22]. Combining technologies of HP and TEG, an innovative waste heat recovery and utilization system (WHRUS) has been designed, built and tested. The importance of this work stems from a change in approach towards the recovery of the energy produced by combustion while enabling control and suppression. Given that nearly one billion tons of coal combusts underground annually worldwide, releasing heat that could potentially generate almost 1000 GW electricity (the current nuclear power and hydropower capacity is currently 400 GW and 900 GW, respectively [17]), achieving any form of energy recovery will be a very positive outcome. .

2. Experiment and methodology

2.1 Experimental background

The Sandaoba coal fire zone is situated in the Midong District of Xinjiang, China (coordinate is E87º25′27″, N43º47′41″). It contains two sub zones oriented in the east-west direction and with the total area of 599, 225 m^2 (A_T). The coal seam is shallow and inclines steeply towards the northwest at an angle of 79-80°. The coal seam is composed mainly of bituminous thermal coal, which is prone to combust spontaneously with a short ignition delay (3-5 months). The sub-surface coal fires are generally found between 70 to 85 m deep, and the maximum burning depth recorded was approximately 191 m. The high temperature spots are randomly distributed towards the west side of the site, and coincide with where the majority of the collapses/pits and fissures are observed.

Fig. 1 Engineering demonstration base (b) for thermal utilization of coal fire underground in Xinjiang, China. And infrared images of a single apparatus (c) and group facilities (a).

The experimental site (35 m×15.5 m) was placed in the western end of the coal fire zone. See the in-situ images of facilities and site in Fig. 1. The surface temperature measured ranged between 25 °C to 70 °C. The burning coal was identified to be between 80 m and 100 m deep and the maximum temperature measured in the boreholes was in excess of 350 °C. The terrain at the site was mostly flat with a consistently high heat flow emerging from the ground which ranged from 10^2 to 10^3 W/m^2. The WHRUS can be directly inserted into the boreholes (Ø132 mm) originally used for firefighting e.g. water and slurry injection. Other devices like radiators and inverters were placed in the warehouse to quantify performances on both heating supply and power generation.

2.2 Apparatus and system

The Waste Heat Recovery and Utilization System (WHRUS) consists of a heat extraction module (HEM), a thermoelectric generator module (TEGM) and cooling module (CM). The arrangement is depicted in Fig. 2. The HEM continuously extracts thermal energy from the coal fire beneath the surface. Associated with the TEGM, the waste heat is converted into the electric power. Meanwhile, CM absorbs the majority of heat to strengthen heat dissipation of TEGM, which is circulated to supply indoor heating.

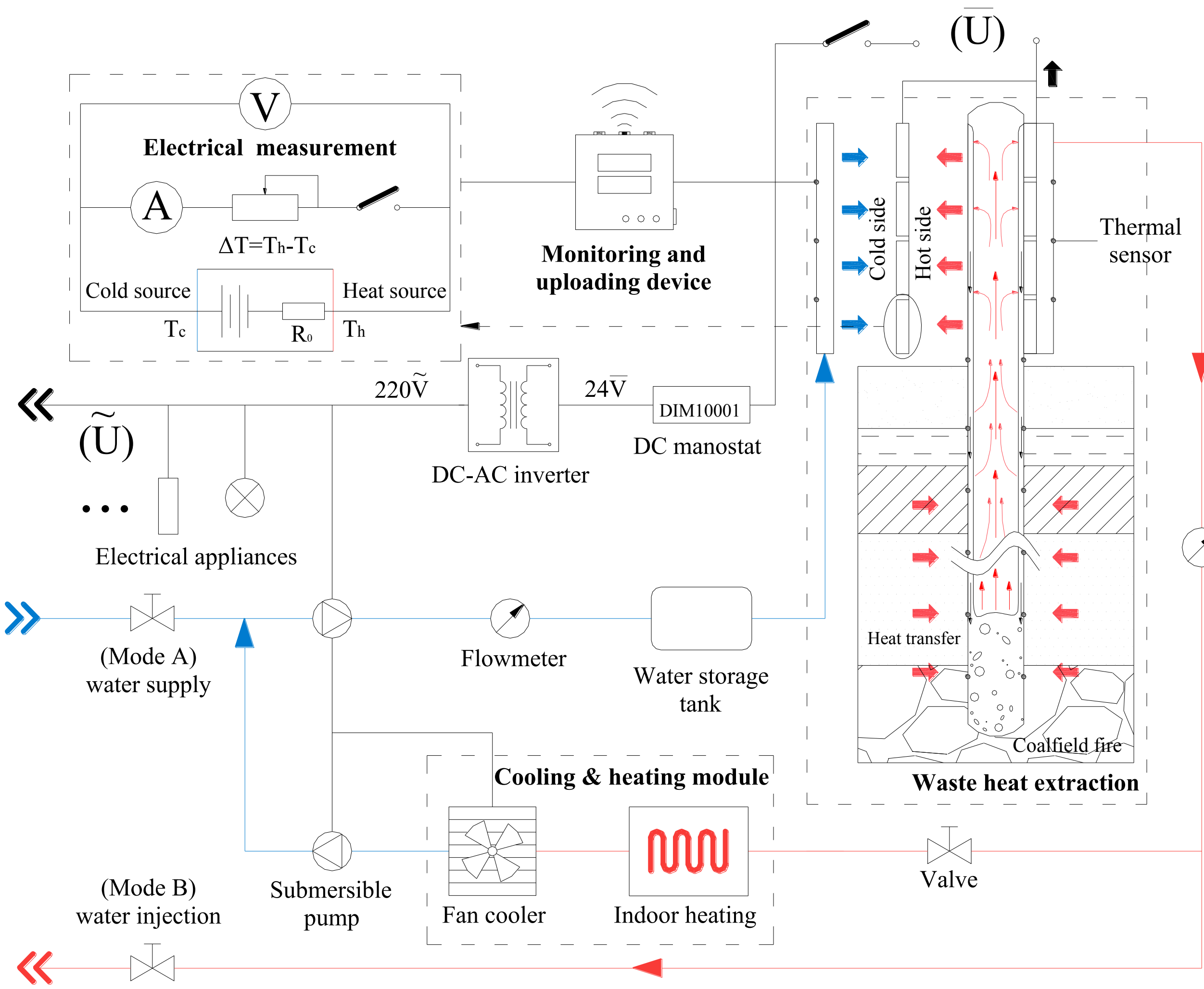

Fig. 2 The composition and principle of WHRUS.

Heat extraction module (HEM)

The gravity heat pipe (GHP), referred to here as the closed loop two-phase thermosiphon (CLTPT), is the core component of the HEM. Its primary purpose is to capture heat. Fig. 3 shows a model of the HP principle. The GHP is a sealed container that transfers heat via the change of phase of an inner working fluid. Along the axial direction, the GHP is divided into three sections of evaporator, adiabatic section, and condenser. When heated in the evaporator (underground), the working fluid/medium vaporizes and migrates upwards into the condenser (surface) where the steam condenses as the temperature decrease. The condensation releases latent heat of vaporization, which is absorbed and transmitted by CM's cooling circuit. Finally, the fluid condensate falls back to the evaporator section by gravity [23]. Thereupon a continuous cycle is developed where the two-phase transformation transfers heat from the bottom to the top of the GHP .

Carbon steel is selected as the tube materials for the HPs to maximize efficiency, safety and economy. Thermal sensors were evenly distributed along the internal and external walls of the HEM to measure temperatures of the different sections of the HP. 10 novel ultra-long-gravity HP devices for normal temperature (50-300 °C) were originally installed. The technical parameters of HPs are presented in Table 1. All the design, manufacture and testing procedures of the GHPs were in strict accordance with the technical requirements of the relevant standards (GB/T 9082.1-201, GB/T 14812-2008 and GB/T 14813-2008).

Table 1 Key design parameters of GHP.

Total length	15.4 m	
Filling ratio	25%	
Vacuity	-10^{-2} MPa	
Working fluid	Distilled water	
Tube material	Seamless boiler steel	
Adiabatic section	Length	0.1 m
Condenser section	Length	3.3 m
	Internal diameter	189 mm
	External diameter	222 mm
Evaporation section	Length	12 m
	Internal diameter	83 mm
	External diameter	95 mm

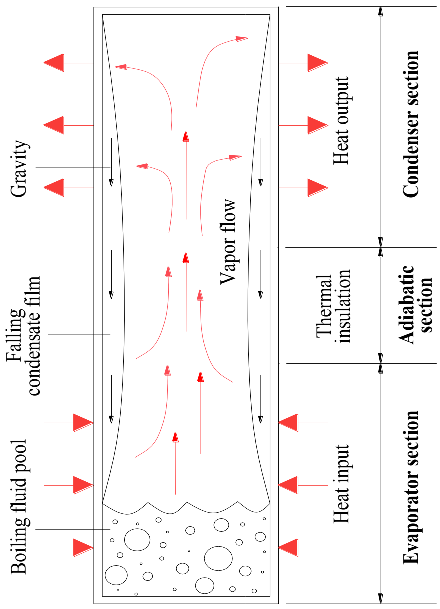

Fig. 3 Schematic of HP principle and process.

Thermal electric generator module (TEGM)

The waste heat extracted from boreholes was directly converted into DC power by the TEGM. Then it supplied power to various appliances after DC-AC conversion. Fig 4 (a) is the schematic diagram of the power generation mode based on the Seebeck effect [41]. When two heterogeneous conductors (P-N type semiconductors) are connected and temperature difference occurs at the two joints, a direct current is produced in the closed loop. The PN junction is formed by series of n/p-type legs made from an alloy of Bi_2Te_3. A plurality of PN junctions are further connected in series to constitute a thermoelectric power generation device (PGD) in Fig. 4 (b). Commercial PGD of TEG1-241-1.4-1.2 was selected and loaded on TEGM with the maximum allowable operating temperature at 200°C.

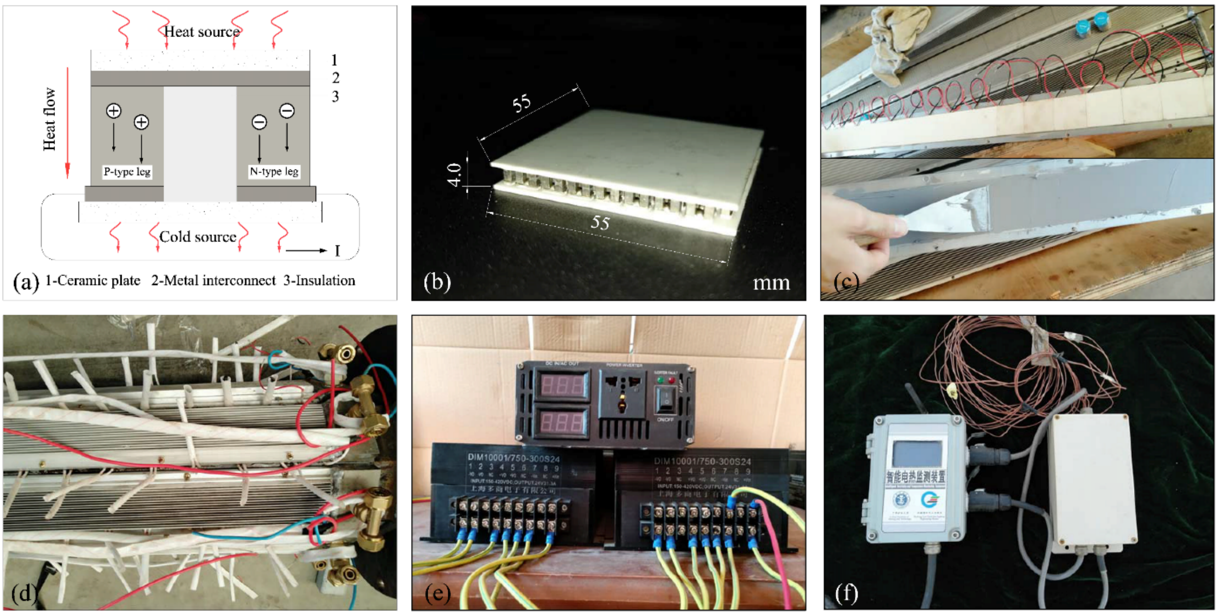

Fig. 4 TEGM: (a) The PN junction formed by connections of n/p-type legs; (b) PGD used for the research; (c, d) PGDs connected and assembled electrically in series and coated with silicon grease; (e) 24V DC manostat and 220V AC inverter; (f) Intelligent electric and thermal monitoring device.

TEGM actually is a power-generation assembly supplied with multiple PGDs that connected in series and parallel. Each TEGM has 400 pieces of PGDs attached to the exterior eight planes of octagonal column in the condenser section. Each plane is affixed with a row of PGDs in 50 chips connected electrically in series as described in Fig. 4 (c, d). And the hot side of the PGD faces inward to the heat pipe, while the cold side is adhered to the square aluminum sheet of the CM. To reduce the contact thermal resistance (>2 W/m·K), a silicon grease is used to coat both interspaces of the PGD. With the heat source and cold source provided by HEM and CM respectively, a stable temperature difference is formed. This promotes thermoelectric conversion. However, the power from TEGM still needs to be regulated to a stable DC voltage of 24V (DIM10001/750-300S24). And the 220V AC power supply could be available through the transformer-module XP665 inverter in Fig. 4 (e).

Cooling (Heating) module

The majority of the heat is absorbed by the cooling module (CM) to enhance efficiency of TEGM while also offering a valuable heating source for indoor warming. The CM is mounted on the cold side of PGD on TEGM, which is comprised of cooling square-fin aluminum sheets, submersible pumps (ZQB5X6-24), flow meters, storage tanks, radiators and water pipelines.

To reduce water consumption, the water delivery mode of CM can be changed from season to season. The cooling water in summer (Mode A) is from water for fire-extinguishing (15 m^3/h). After being precipitated and filtered, this water (15°C) is pumped to WHRUSs for heat dissipation of TEGM, then directly discharged (30°C) into the nearby boreholes again for fire-fighting injection. In winter (-10 °C average), fire-extinguishing work stops and water delivery is cut off since the pipeline freezes. Heating module (HM) starts to operate. Therefore, the method of water self-circulating & air-fin cooling (Mode B) is adopted for both heating and cooling, as is shown in Fig. 2. The water is pumped out of the tanks and flows to the aluminum sheets where heat convection dissipates the heat from the TEGM. This water is subsequently heated (>65°C) then transported through pipelines to the household radiators for indoor heating. After that the water is cooled down by the fan radiators outdoors. The cold water flows back to complete the circuit of the cooling-heating mode (Mode B).

2.3 Experimental methods and process

Quantification of heat extraction and utilization can be delivered by measuring the in-site thermal data: temperatures, heat flux and infrared images. Different types of K-type thermocouple and thermometers (0.01℃) were used to measure temperatures. To investigate the temperature distribution versus depth, temperatures were vertically placed in-depth every five meters for all boreholes. To establish the field-scale temperature distributions, images obtained with an infrared imager (FLIR-T610) and processed with FLIR QuickReport 1.2 SP1 were used. The field survey of heat flux measurement was made with the portable single-point heat flow meter JTR01. See points arranged on a triangular geometry in Fig. 7. It was typically started with grid mapping where flow measurements were taken at the grid nodes. Another set of measurements was added to those represented points on thermally active vents. Special software Surfer [46] was used to draw the thermal topographic map (1:1) using the heat flux and GPS data (by eTrex 201X). Through finite element analysis of Matlab [47], we could finally estimate the resource storage of waste heat for the whole selected fire area. To study the thermodynamic process of WHRUS, some characteristic parameters e.g. velocity and pressure of exhaust gas are necessary. Their time evolution was measured by means of a DFA-III anemometer, Pitometer (L-500) and *U* tube manometers.

In Fig.2, the electrical performance of WHRUS could be reflected by long-term monitoring of the open circuit voltage (U_{ocv}) and short circuit current (I_{scc}). Applying the innovative intelligent measuring device CUMTET-18I in Fig. 4(f) and the VC890D multimeter, the operating temperatures (Fig. 10) and electrical output data (Fig. 11) could be observed and uploaded every day automatically, which is convenient to constantly monitor the stability and efficiency of each WHRUS. The inside/outside temperature and heat flux from radiators were also monitored for over a month. And the flowmeter (PST-LD-DN65) recorded water flows from branches of the WHRUS pipeline. After that, the warming efficiency and quality were able to obtained for district heating evaluation.

Finally, with the field surveys and WHRUS measurements, a model is is developed to estimate the large-scale extraction and utilization of the waste heat in the coal fire zone.

3. Theory

3.1 Estimation of the waste heat resource

For boreholes, steady-state thermometry is suggested to obtain thermos-physical features of the fire zone and to study geothermal field. The geothermal gradient is used to analyze the temperature distribution versus vertical depth, which is derived from regression of

$$grad\ T = \lim_{\Delta H \to 0} \left(\frac{\Delta T}{\Delta H} \right) = \frac{\partial T}{\partial H} \tag{1}$$

where $\partial T/\partial H$ denotes the derivative of the temperature in the depth direction.

The heat flow (heat flux) indicates the amount of heat dissipation from the surface. Provided the thermal anomaly area S and the heat flux q in-site are known, the total heat released from coal-fire underground can be estimated via:

$$Q_L = \iint_S q(x, y)dxdy \approx \sum_i \sum_j q(x_i, y_i)\Delta x_i \Delta y_i \tag{2}$$

3.2 Thermodynamic model of WHRUS

The heat-transfer model proposed for WHRUS enables the determination of the thermal resistances of each part and to systematically quantify the heat extraction. The main assumptions of the model are as follows: (1) The system is closed therefore there is only heat exchange but no mass exchange between the cold source and heat source in HEM. (2) The thermophysical properties of the fluid are independent of temperature, and all thermal phenomena are regarded as steady processes. (4) All coefficients used for empirical correlations are determined with the data and used only as a best estimates for any real system. (5) The inside of HP is ideally isothermal, the steam is always saturated and has a small Reynolds number. (6) Radiative heat transfer is simplified to the steady radiation between gray bodies. (7) The average shallow temperature (above -15 m) is assumed to be a constant.

Allowing for these hypotheses, the heat-transfer process can be characterized by the thermosphysical model and thermal network in Fig. 5. Representative values will be correlated from data to calculate the thermal resistances of the individual units in Table 2.

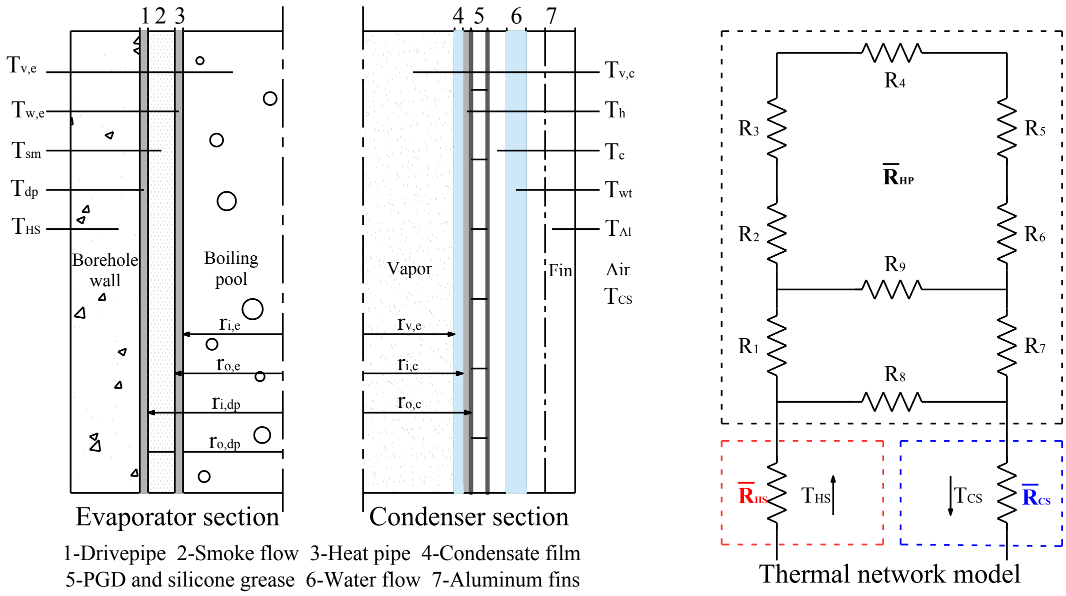

Fig.5 Equivalent heat transfer model and the thermal resistance network of WHRUS.

Table 2 Expressions and deduction of sub-thermal resistances.

$R_1=\dfrac{ln(r_{o,e}/r_{i,e})}{2\pi L_e\lambda_{w,e}}$	$R_{cond1}=\dfrac{ln(r_{i,dp}/r_{o,e})}{2\pi L_e\lambda_{sm}(1-\beta)}$
$R_2=1/(2\pi r_{i,e}L_e\alpha_e)$ [48]	$R_{cond2}=\dfrac{ln(r_{o,dp}/r_{i,dp})}{2\pi L_e\lambda_{dp}\beta}$
$R_3=\dfrac{R_gT_v^2\sqrt{2\pi R_gT_v}}{2h_{fg}^2P_v\pi r_{i,e}L_e}$ [49]	$R_{conv}=1/(2\pi r_{o,e}L_e\alpha_{sm})$
$R_4=\dfrac{8R_g\bar{L}vT_{v,e}^2}{\pi r_{i,e}^4h_{fg}^2P_v\rho_v}$ [50]	$R_{radi1}=\dfrac{10^8(T_{sm}-T_{w,e})}{C_{sm}A_1(T_{sm}^4-T_{w,e}^4)}$
$R_5=\dfrac{R_gT_v^2\sqrt{2\pi R_gT_v}}{2h_{fg}^2P_v\pi r_{i,c}L_c}$	$R_{radi2}=\dfrac{10^8(T_{dp}-T_{w,e})}{C_{dp}A_2(T_{dp}^4-T_{w,e}^4)}$
$R_6=1/(2\pi r_{i,c}L_c\alpha_c)$ [51]	$R_{TEG}=\dfrac{T_h-T_c}{P_{max}}$
$R_7=\dfrac{ln(r_{o,c}/r_{i,c})}{2\pi L_c\lambda_{w,c}}$	$R_{air}=1/\left[\alpha_{air}\left(A_0+\eta_{fin}A_{fin}\right)\right]$
$R_8=L_{e+o}/[\pi\lambda_{w,e}(r_{o.e}^2-r_{i,e}^2)]+L_c/[\pi\lambda_{w,c}(r_{o.c}^2-r_{i.c}^2)]$ [52]	$R_{wt}=1/(\alpha_{wt}A_{wt})$
$R_9=L_{e+o}/[\pi\lambda_{f,e}(r_{i,e}^2-r_{v,e}^2)]+L_c/[\pi\lambda_{f,c}(r_{i.c}^2-r_{v.e}^2)]$	$\overline{R}_{HS}=(T_{HS}-T_{w,e})/\sum(\Delta T/R)_{HS}$
$\overline{R}_{HP}=\dfrac{[R_1+R_9\cdot\sum_2^6R_i/(R_9+\sum_2^6R_i)+R_7]\cdot R_8}{[R_1+R_9\cdot\sum_2^6R_i/(R_9+\sum_2^6R_i)+R_7]+R_8}$	$\overline{R}_{CS}=(T_c-T_{CS})/\sum(\Delta T/R)_{CS}$
Notes:	R_{cond1} (R_{cond2}): the contact thermal resistance of smoke (drivepipe);
R_1 (R_7): the wall-radial conduction resistance of the evap (cond) section;	R_{conv}: the convection thermal resistance of smoke;

R_2 (R_6): the wall-film convention resistance of the evap (cond) section;	R_{radi1} (R_{radi2}): the radiation thermal resistance of smoke (drivepipe);
R_3 (R_5): the thermal resistance of vapor-liquid evap (cond);	R_{TEG}: the thermal resistance of TEG;
R_4: the axial thermal resistance of vapor flow;	R_{air}: the convection thermal resistance of air;
R_8 (R_9): the axial conduction resistance of the wall (film);	R_{wt}: the convection thermal resistance of cooling water;
$\overline{R}_{HP}$: the equivalent thermal resistance of thermosyphon (HP).	$\overline{R}_{HS}$ ($\overline{R}_{CS}$): the equivalent thermal resistance of heat (cold) source.

3.3 Quantifying the waste heat extraction

Through process of heat transfer involving conduction, convection and radiation, the coal-fire geothermal energy is extracted from heat source of single borehole, which can be theoretically calculated by Eq. (3):

$$Q_{HS}=\left(T_{HS}\text{-}T_{w,e}\right)\left(R_{cond1}{}^{-1}+R_{cond2}{}^{-1}+R_{conv}{}^{-1}+R_{radi1}{}^{-1}+R_{radi2}{}^{-1}\right) \tag{3}$$

The heat moves to the HP condensation section by phase changing, and is continuously transmitted since water/air cooling and TE conversion. The theoretical heat transfer to the cold source can be derived by:

$$Q_{CS}=\frac{T_c\text{-}T_{wt}}{R_{wt}}+\frac{T_{Al}\text{-}T_{CS}}{R_{air}}+\frac{\left(\sum U_{TEG}\right)^2}{4\sum r_{TEG}} \tag{4}$$

while the practical heat absorbed by cooling source can be equivalently totted up with the energy converted.

$$Q_{CS}{}'=\rho_{wt}q_{wt}C_{p,wt}\Delta T_{wt}+(E_{ocv}I)_m+q'A_{air} \tag{5}$$

3.4 Thermal energy conversion and utilization

Thermal energy can be transformed into electric energy by TEGM via Seebeck effect. The thermal electromotive force E is proportional to the temperature difference between the hot end and cold end.

$$E=S_e(T_h\text{-}T_c) \tag{6}$$

Efficiency of TEG can be approximated by the following correlation [53]:

$$\eta_{max}=\frac{T_h\text{-}T_c}{T_h}\cdot\frac{\sqrt{1+Z\overline{T}}\text{-}1}{\sqrt{1+Z\overline{T}}+T_c/T_h} \tag{7}$$

where $\overline{T}=(T_h\text{-}T_c)^{-1}\int_{T_c}^{T_h}TdT$, $Z=\left(\alpha_p\text{-}\alpha_n\right)^2/\left(\sqrt{\lambda_p\rho_p}+\sqrt{\lambda_n\rho_n}\right)^2$, and $Z\overline{T}$ is the dimensionless figure of merit on average to determine whether the TE characteristic is good or not [54]. In contrast, the maximum actual efficiency can be measured at the peak of power output on which the optimal electric load is set.

$$\eta_{max}{}'=\frac{P_{max}{}'}{Q_{CS}{}'}=\frac{E_{ocv}{}^2/4r_{max}}{Q_{CS}{}'} \tag{8}$$

In addition to electrical conversion, most of the heat extracted is directly utilized for indoor heating, which is hereafter quantitatively expressed by heat released from hot water:

$$Q_{wt}=\rho_{wt}q_{wt}C_{p,\,wt}(T_{in}\text{-}T_{out}) \tag{9}$$

4. Result

4.1 Assessment of waste heat resource

4.1.1 Geothermal analysis

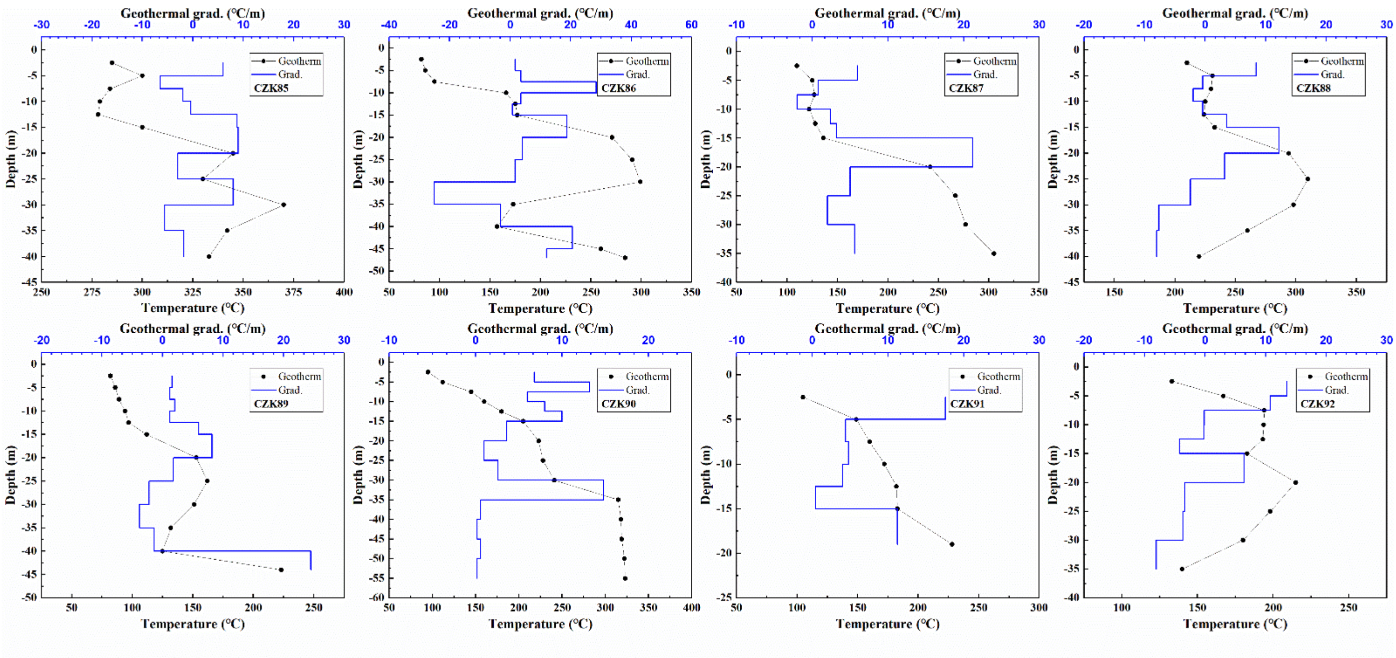

Fig. 6 The measurement of temperature versus depth with the thermal gradient.

The temperature distribution in boreholes is reflected by the temperature-depth curve plotted in Fig. 6, and the geothermal gradient can be obtained according to Eq. (1). At depths less than -20 m, the temperature presents an overall upward trend as the depth increases. Between -20 m and -25 m, the thermal conductivity of the rock is small, due to the crumbling passages of the mudstone or siltstone, and heat is accumulated. The accumulated heat forms thermal deposits, causing a significant temperature increase (the maximum temperature). Deeper, into layers with higher thermal conductivity, the temperature decreases gradually. Until depths below -40 m where the temperature rises sharply again because boreholes (CZK 89, 86 and 90) most likely have penetrated deeper cavities or cracks. None of the curves show typical linear-conductive distributions commonly associated to geothermal temperatures. Temperature fluctuations and significant undulations of the corresponding geothermal gradient can be potentially associated to the fracture of strata, the development of fissures and the extreme layered structure of the coal seam. Therefore, it is concluded that the coalfield-fire waste heat in this area can be defined as the convective-conductive composite geothermal resource.

4.1.2 Heat flow analysis

The waste heat from underground coal fire is mainly dissipated through the surface, which can be measured by the value of the surface heat flux. The entire experimental base was covered with representative points to observe the dynamic surface heat flow for extended periods of time. The geographical layout of survey points is presented n Fig. 7. And the results are analyzed by the following three methods.

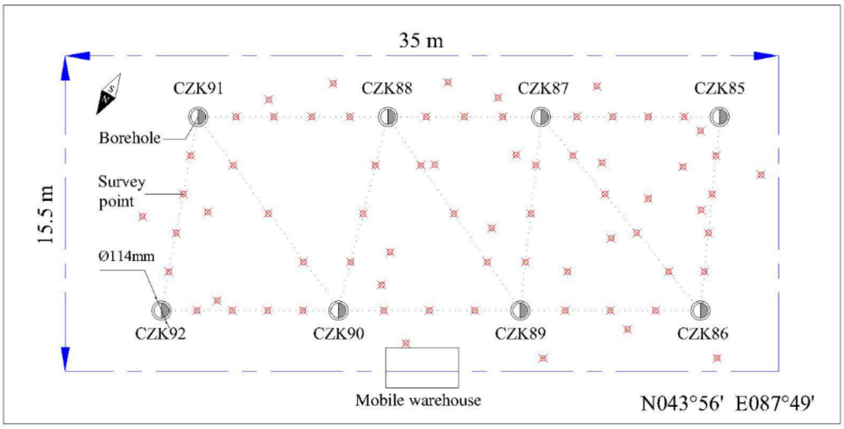

Fig. 7 The geographical layout of the equipment and measuring points.

(1) Data processing of individual heat flow value: the sample average and variance statistics is adopted for multiple readings of each point to obtain the effective heat flow, thereby reducing the impact of measurement errors induced by environmental interference on the temperature such as wind, sunlight etc.

(2) Statistical analysis on subgroup heat flow data: the statistical description in Table 3 indicates that the heat flow of the thermal recovery ranges from 63 to 1250 W/m^2. The mean value is about 536 W/m^2, nearly hundredfold higher than normal levels measured for the local area (38 to 82 W/m^2). The frequency distribution statistics for all heat flow in Fig. 8 shows the overall trend of heat flow data that generally follows a normal-like distribution: q~N (649.1258, 714.8336^2), and the parameters fitted by the normal curve are presented in Table 4. The highest frequency of heat flux occurs in the range of 430~570 W/m^2 which is in the same range as the mean value. The expected value (649 W/m^2) is slightly higher than that range, owing to the uneven data

grouping and improper layout of some measuring points. From the analysis on the total heat flow level and differential distribution, it can be inferred that the local geothermal energy supplied by the underground coal fire is of very significant magnitude and therefore suitable to be recovered and reutilized.

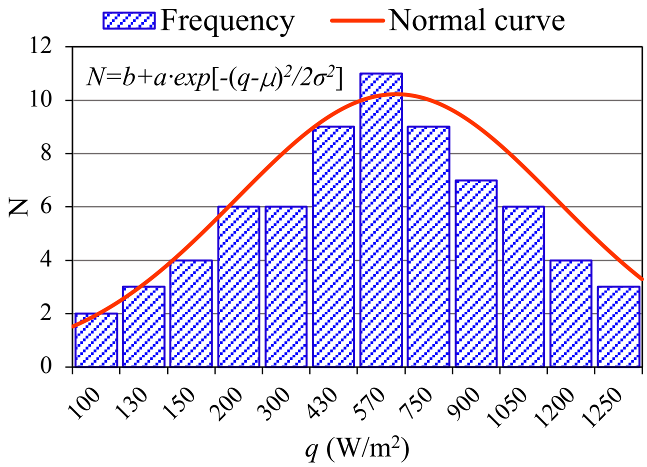

Fig. 8 Histogram and normal distribution of heat flow.

Table 3 Statistical description of heat flow value.

Count (N)	Mean	Geometric mean	Standard deviation	Variance	Min	Medium	Max	Confidence (95%)
70	536.253	422.357	332.637	110647.1	63.013	490.900	1249.441	79.314

Table 4 The fitting parameters of the normal distribution curve.

Fitting model	b	μ	σ	a	R^2
GaussAmp	0.2175	649.1258	714.8336	10.0049	0.9091

(3) Numerical resource estimation of waste heat reservoir: surface heat flux is numerically equal to the product of the temperature gradient and thermal conductivity. It is a comprehensive thermal parameter to reflect the combustion severity and heat exchange through the ground. Combined with the relevant geo-exploration, a geological-thermal map can be drawn to identify spatial variations and local anomalies of the heat flux. First, it is necessary to summarize the heat flux differences and geological distribution trends in the graph. The iso-domain of the heat flux in Fig. 9 (a) exhibits a scattered distribution with substantial spatial difference in both the lateral and longitudinal direction. It is obvious to see considerable undulations among the isosurface in Fig. 9 (c), where the heat flux values are extremely uneven. Generally, the temperature and heat flux gradients are larger in the regions with small thermal conductivity. The initial heat flux data and contour diagram in Fig 9 (a, c) show significant fluctuations, discontinuities and divergences, leading to errors of significant

magnitude when estimating the thermal output. For this reason, numerical processing by means of interpolation, inversion and correction is performed to correct for missing data points and significant deviations of the heat flux. Based on the thin-plate splines method, the data matrix of the measured heat flux can be obtained. The whole area is finally divided into 17360 grids (0.25 m×0.125 m), as shown in Fig. 9 (b, d).

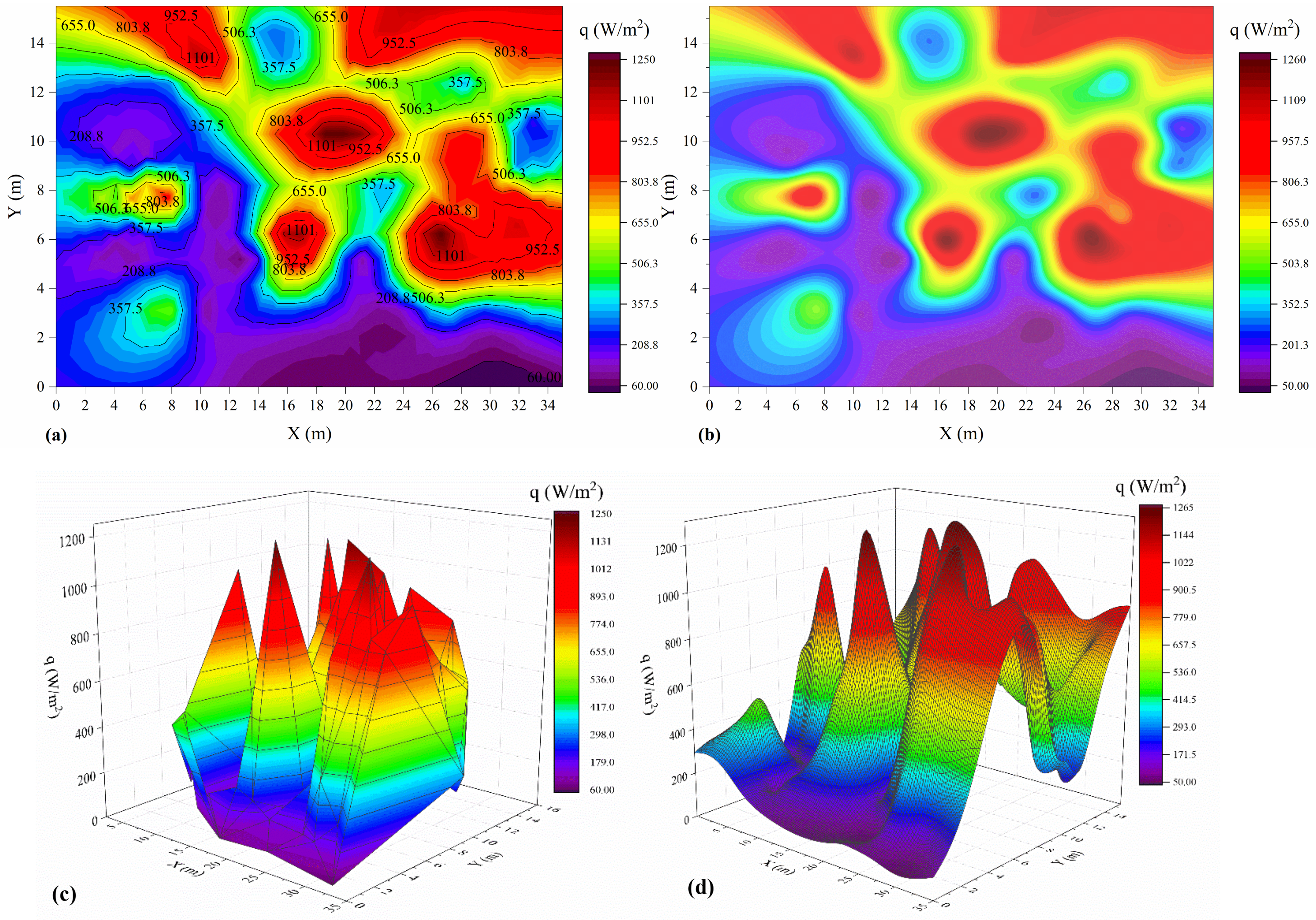

Fig 9 Geographic-thermal distribution map of heat flux: comparisons on the initial (a, c) and the corrected (b, d) contour diagrams of the 2D/3D distribution.

After the meshing and fitting corrections, according to the numerical finite element processing with Eq. (2), the heat loss from the entire experimental site is 268.27 kW while the average heat flux (q_{ave}) is 494.507 W/m^2. The total waste heat of 368.13 kW can be extracted from 8 holes where the thermal output per hole is 46.016 kW calculated in Chapter 4.2. The sum of surface heat loss and the heat extracted from boreholes is approximately the total waste heat reserve, namely 368.13+268.27=636.4 kW, with a thermal recovery rate of 368.13÷636.39=57.85%.

The measurement result implies the high level of overall heat flux in the area, the distribution of which is yet uneven due to the coalfield geological and burning conditions. The numerical estimation further demonstrates that the waste heat resource of coal fire in this region has possessed both a large amount of geothermal energy and high potential for waste heat recovery.

4.2 Thermal performance of WHRUS

4.2.1 Heat transfer characteristic

Isothermality and conductivity are crucial criteria to appraise the heat-transfer characteristic of HP. Fig. 10 (a) reveals the monthly variation of temperature versus time along the axial positions of HEM. The temperatures of the same position change periodically around a certain level. Except for sudden changes affected by extreme weather on a few days, temperature change is small on the same position with the average amplitude less than 6 °C. In different parts of the condensation section but for the same time, the average temperature difference does not exceed 5 °C either. From temperature monitoring, it can be inferred that WHRUS have displayed the excellent isothermality and stability, which also indicates that the system is running well and heat transfer on waste heat extraction keeps stable.

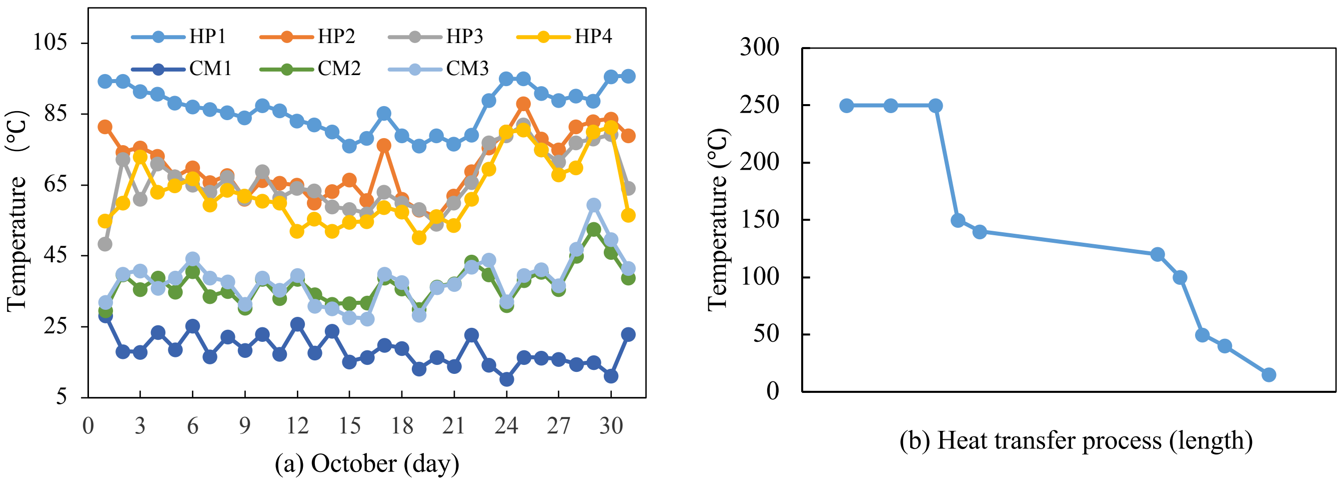

Fig. 10 (a) Monthly temperature monitoring on different positions of WHRUS. HP1-HP4 is the smoke outlet, adiabatic section, the bottom and top ends of HP, respectively. CM1-CM3 denotes the bottom, middle and upper part of CM, respectively. (b) Temperature drops of the axial and radial distribution along HP during heat transfer.

Moreover, the HP thermal conductivity can be reflected by the temperature drop and thermal resistance. Referring back to the equivalent formulas in Table 2, the thermal resistances of each unit of WHRUS are derived in Table 5. Among the sub-thermal resistances, the values of R_3 and R_5 are relatively large, together accounting for more than 65% of the total resistance ($\overline{R}_{HP}$). It is also found in Fig. 10 (b) that the temperature usually decreases the most at the heat exchanging interfaces between the heat/cold sources and HP walls, since the much larger resistances of R_3 and R_5. At last, compared with the empirical magnitudes of resistances in previous studies [49], the theoretical resistances of R_3, R_4 and R_5 are relatively larger. And that is the main factor to increase the overall resistance ($\overline{R}_{HP}$) and temperature drop.

Table 5 The results and comparison of sub-thermal resistances.

HP resistance	Result	Empirical magnitude	External resistance	Result
R_1	3.56921E-05	10^{-1}	R_{cond1}	0.0552003
R_2	0.0005277	10^{-4}	R_{cond2}	0.0019252
R_3	0.0011092	10^{-5}	R_{conv}	0.0057746
R_4	0.0003579	10^{-8}	R_{radi1}	0.0461631
R_5	0.0020801	10^{-5}	R_{radi2}	0.0107406
R_6	0.0006888	10^{-4}	$\boldsymbol{\overline{R}_{HS}}$	**0.0021732**
R_7	9.94586E-05	10^{-1}	R_{wt}	0.0006089
R_8	153.33446	10^{2}	R_{air}	0.0142330
R_9	1.64230E+04	10^{4}	R_{TEG}	0.0756920
$\boldsymbol{\overline{R}_{HP}}$	**0.00489877**	10^{-3}	$\boldsymbol{\overline{R}_{CS}}$	**0.00195511**

4.2.1 Thermal balance analysis

The imbalance of heat budget often appears in industrial heat pipe exchanger for waste heat recovery. Therefore, it is particularly essential to pre-examine the thermal equilibrium on heat extraction (input) and transmission (output) for evaluating heat-transfer performance. (Here by taking the WHRUS in borehole CZK90 as an example)

Firstly, the resultant values of resistance in Table 5 are substituted into Eq. (3), and each part of the heat source is calculated then summed up to obtain the input of heat source $\sum(Q)_{HS}$ shown in Table 6. Among these heat branches, the borehole waste heat is mainly transferred to the evaporator section by smoke convection Q_{conv} and wall conduction Q_{cond2}, both contributing to almost 70% input of the total heat. As for the waste heat output, the heat actually received by the cooling system, is the consequent sum of the heat transfer, heat conversion and heat dissipation, which directly reflects the comprehensive utilization and transformation of coal fire thermal energy. In like manner, Eq. (4) adopt resistances of the cold source in Table 5 to deduce the theoretical thermal output $\sum(Q)_{CS}$. The partial energy conversion on field is measured listed in Table 7 (b) to obtain the actual heat output $\sum(Q')_{CS}$ using Eq. (5), as presented in Table 7 (a).

Table 6 The composition of heat input per single borehole (heat source).

Q_{cond1}	Q_{cond2}	Q_{conv}	Q_{radi1}	Q_{radi2}	$\sum(Q)_{HS}$ (kW)
1.8116	15.5828	17.1441	2.1662	9.3105	46.0152

Table 7 (a) Theoretical and actual composition of heat output per single borehole (cold source).

Theoretical heat (kW)	Q_{wt}	P_{TEG}	Q_{air}	$\sum(Q)_{CS}$
	41.0588	0.6606	1.7565	43.4759
Actual heat (kW)	Q_{wt}'	P_{TEG}'	Q_{air}'	$\sum(Q')_{CS}$
	39.5332	0.5488	2.43	42.5120

Table 7 (b) Energy conversion measurement of actual heat output.

T_{wt}	T_{wt}'	q_{wt}	ρ	C_p	E_{ocv}	I	q'	A_{air}
14.7	39.8	3.778E-04	996.7	4.183	307	1.788	225	10.8

By comparing the thermal input with the thermal output, it is found that there is an asymmetry of heat budget in WHRUS. $\sum(Q)_{HS}$ is slightly larger than $\sum(Q)_{CS}$, which the thermal deviation of the balance (heat loss rate) is $1-\sum(Q)_{CS}/\sum(Q)_{HS}=5.5185\%$. In addition to the defects of facility design and thermal circulation, the heat loss along the transfer process is also one of the key factors to cause the nonequilibrium. It is also noticed that the actual heat outputs (Q_{wt}' and P_{TEG}') are smaller than the theoretical ones (Q_{wt} and P_{TEG}) but the situation is opposite for the heat dissipation of air measured by heat flux ($Q_{air}'>Q_{air}$). Since the presumptions and conditions are simplified in thermal operation, representation of a system using resistance method may over-estimate the total heat output in reality ($\sum(Q)_{CS} >\sum(Q')_{CS}$).

By the analysis on the thermal balance, the recovery rate of waste heat per hole is $\sum(Q)_{CS}/\sum(Q)_{HS}=94.481\%$. The low thermal resistance and strong thermal exchange both indicate the excellent heat transfer performance of WHRUS, even though there is still a small deviation between results of the proposed model and in-site thermal measurement.

4.3 Waste heat energy utilization and conversion

Waste heat utilization in the fire zone includes two means of direct heating supply and indirect thermoelectric (TE) conversion. The operation of TE conversion is automatically observed by intelligent measuring equipment, and the monthly change of power generation is recorded in Fig. 11 (a). The temperature difference of 50 °C is able to produce the maximum power output of 1586.91 W, while the corresponding U_{ocv} and I_{scc} is 507 V and 3.13 A, respectively. The dynamic electrical values remain stable throughout the month, and the average power generated per hole is above 960 W. The peaks are noticed on cold days of October when borehole pressure was increased to strengthen flow for smoke convection. Then the temperature difference was increased between the hot and cold ends of TEG, eventually leading to the improvement of TE conversion.

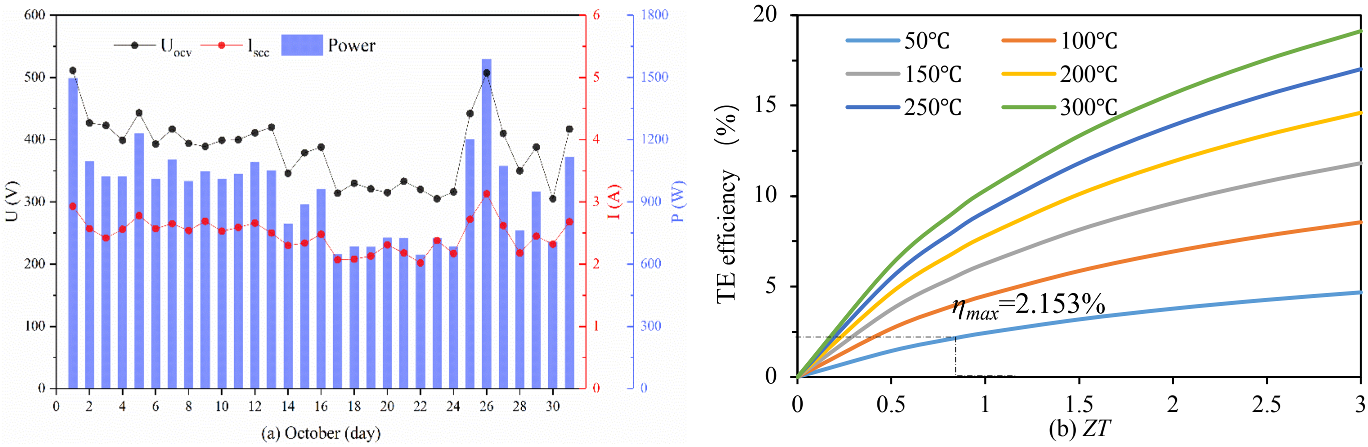

Fig. 11 (a) Monthly monitoring of single-hole (CZK90) power generation; (b) TE efficiency as a function of ZT_{ave} at various temperature differences.

After determining the electric quantities, the actual and theoretical power generation efficiency of the equipment and TE materials were separately derived. See in Table 8. According to the reference [55], the physical properties of the P-N type semiconductor were determined at first, then to derive the $Z\bar{T}$ of the experimental TE material as 0.841748 by Eq. (7). As shown in Fig. 11 (b), the TE efficiency is increasing as a function of $Z\bar{T}$ and temperature difference. The theoretical conversion efficiency of Be_2Te_3-based material is 2.153% at the temperature difference of 50 °C. By using Eq. (8), the theoretical (η) and the actual (η_{max}') TE efficiency of the WHRUS were figured out but smaller with 1.519% and 1.291% respectively. They are much smaller compared with the traditional Carnot cycle efficiency (35%), which is also a general deficiency faced by thermoelectric field. Even despite the currently low TE efficiency, the waste resource still remains tremendous in amount that is cheap and easy to acquire. Furthermore, TE technology has better adaptability to complex working conditions in coalfield. Contrasted with other conventional geothermal power generation systems, the small-scale movable TE systems are more economical especially for the short term fire period. All of these renders TEG a superiority technology to apply on energy conservation for waste heat harvesting.

Table 8 Material properties and thermoelectric efficiency.

TE properties	p-type	n-type	TE efficiency	
S_e	1.4693E-04	-1.5382E-04	$\eta = P_{TEG}/Q_{CS}$	1.519%
K	4.7273E-06	4.39396E-06	$\eta_{max}' = P_{TEG}'/Q_{CS}'$	1.291%
λ	2.07614	2.02410	η_{max}	2.153%
Z	2.4188E-03		η_{comm}	10%
$Z\bar{T}$	0.841748		η_{carnot}	35%

Table 9 Calculation and measurement parameters of district heating.

$T_{wt,HP}$	$T_{in,ra}$	$T_{out,ra}$	$C_{p,wt}$	$q_{wt,HP}$	$q_{wt,ra}$	q_{radi}	Q_{ih}	Q_{ab}	η_{ih}
17	64	39	4.174	1.161	0.823	220~340	23.617	62.846	37.578%

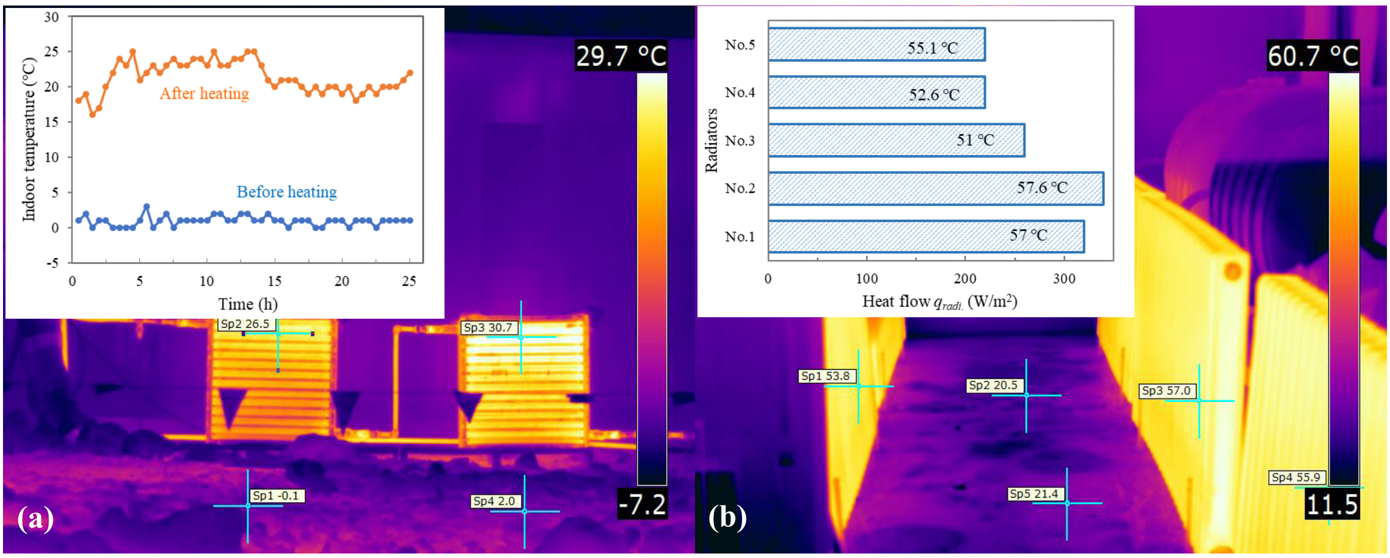

Fig. 12 The infrared images, (a) temperatures and (b) heat flow change of heating supply.

A small amount of the extracted heat is converted into electricity, while more than 90% of the heat (Q_{wt}') is directly absorbed by water through CM, thereby achieving the maximum thermal concentration and heat transfer. Water flows through the CMs in sequence to absorb the heat Q_{ab} (kW) from TEGMs. This hydrothermal resource can provide warmth to the residential area within one kilometer. The cold water returns back to CMs after releasing heat by radiators. Fig. 12 (a) shows the comparison of room temperatures before and after indoor heating in winter. The outdoor temperature is usually below freezing, while it is stable above 20 °C inside. The indoor/outdoor radiators are all operating at the same time. The infrared images, heat flow q_{radi} and temperatures of the radiators are recorded and presented in Fig. 12 (b). Using Eq. (9), the amount of indoor heating Q_{ih} (kW) and the warming efficiency η_{ih} are finally calculated in Table 9. The heating efficiency is not high with only 37.578%. Most of the heat scatters into the air along the way that could not be fully used for heating. Through heating supply, the temperature of hot water is only reduced to 39 °C which can not meet the requirement of the cooling cycle (below 20 °C). So another outside cooling process (air-fans) are added here to assist the second water cooling.

4.4 Estimation of waste heat resource and energy saving

Here we take the western fire field as an example to estimate the overall benefits on waste heat resource, energy saving and economy in Table 10. According to the on-site investigation and report [56]. The area of the western fire area (A_w) is about 443, 588 m^2 in which over 500 holes are designed for fire extinguishing. The duty time is 250 days a year and 8 hours a day. All the intermediate and statistics variables used in the following assessment are resultants derived from Chapter 4.1-4.3.

Table 10 Estimating the overall benefits on waste heat resource, energy saving and economy.

Resource assessment	Total heat reservation (MW/a)	Average heat recovery (%)	Fissure heat loss (%)	Heat recovery (MW/a)
	240.6	57.85	24.41	105.2
resources conservation	Unit heat extraction Q_{CS}' (kW)	Annual heat extraction (kJ)	Vaporization enthalpy (kJ/kg)	Water saving (t/a)
	42.5	1.53×10^{11}	336.19	4.55×10^{5}
	Unit power generation (kW)	Annual electricity generated (kWh)	Electricity charge (USD/kWh)	Financial saving (USD/a)
	1	10^{6}	0.07267 $	72670 $
Regional heating	Unit heat supply (kW)	Total heat supply (kW /a)	Heating load index (W/m^2)	Heating area (m^2 /a)

	15.97	7985.39	60	1.33×10^5

Annotation:

Total heat reservation=$Q_{CS}'\times500+(q_{ave}=0.49451)\times A_w=240.607$ MW /a. Heat loss affected by fissure areas equals to $146297/A_T=24.41\%$. Annual electricity generated=$1\times250\times8\times500=10^6$ kWh. Unit heat supply=$Q_{CS}'\times\eta_{ih}=15.971$ kW. Vaporization enthalpy is the heat absorbed by the water vaporization from 20 to 100 ℃, also equivalent to the heat released from coal fire after cooling.

5. Discussion

In order to shift the thinking of fire control to thermal application, this paper has theoretically and technically discussed the feasibility of waste heat extraction and utilization on coalfield fire. Firstly, the waste heat resource in the coal fire field was comprehensively evaluated. In terms of thermal reserve and spatial distribution, the coal fire geothermal resource in this region is considerable and potential in both exploitation and recovery. From a perspective of theoretical rigor, the paper thus established an equivalent heat-transfer model in accordance with the on-site conditions. The key parameters of heat-transfer operation have also been quantitatively analyzed, such as thermal resistance, temperature drop, heat storage, recoverable amount and extraction efficiency. To put a system of this nature into practice, the WHRUS system was design proving to be im minently suitable for the task.

Through quantitative evaluation of waste heat resource, energy saving and conversion, it can be concluded that the fire area underground possesses an abundance of waste heat resource and superior condition of exploitation and utilization, which could be comparable to the conventional medium-low temperature geothermal resource. Moreover, once the heat is continually removed from the fire zone, the surrounding temperature declines gradually to speed up the control and restoration of coal field fire.

Whereas, certain questions have yet to be studied and solved. First, besides the preliminary thermal evaluation, the corresponding matching and array method of HPs batch should be studied for selecting favorable thermal channels to implement WHRUS. Second, to ultimately reduce the resistance and the thermal loss, the future HP production needs to be further developed in a centralized manner leading t improvements on structure, size, filling rate and materials. Third, for narrowing deviation between the proposed model and practical measurement, it is also necessary to simplify the hypotheses, enrich the resistance network theory and balance the thermal budget as far as possible. Fourth, future research is urgently demanded to improve the efficiency of the TEG system, which can be optimized by specific design and matching on TE facility. It is advised to select the TE material with higher *ZT* value and boost the TEG temperature difference as large as possible. Lastly, more investigations will be carried out to study the influence factors associated to space heating to ultimately improve heating efficiency.

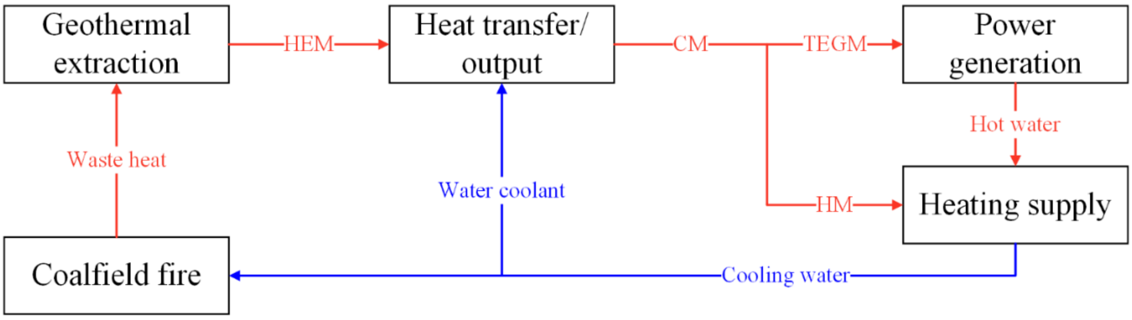

Fig. 13 Technical route for the extraction and utilization on waste heat resource of coal fire.

Using water, also the working medium of HP, as the thermal exchange carrier, the underground coal fire energy recovery and utilization system has exerted multiple functions of heat extraction, thermal transfer, synthetic utilization and conversion, forming an integrated sustainable mode of coal fire extinguishing, waste heat power generation, district heating, energy saving and emission reduction. As is summarized in Fig. 13, the circulation mechanism is committed to maximizing the extraction and utilization of coal fire waste heat energy. More importantly, it has provided a novel concept for the management and restoration of coal-field fires.

The present work can be extended to other areas under similar conditions of waste heat recovery and thermal hazard prevention: for instance, spontaneous combustion in mines, heat elimination of mining waste dumps, prevention and utilization of heat hazard in deep mines, and thermal control and utilization in long-deep tunnels.

6. Conclusions

This paper a sub-surface coal-fire is treated as a shallow geothermal source for energy recovery.A systematic study of how to estimate, recycle, utilize and assess the magnitude of this energy resource is proposed. The thermal evaluation was made by establishing the source of energy, a method to quantify the resource and by conducting a detailed heat transfer analysis. The geo-temperature and geothermal gradient of the borehole do not show the typical linear-conductive distribution trend. Thus, the geo-temperature and geothermal gradient are defined by the combustion process and therefore the energy that can be potentially recovered is defined as the convective-conductive composite geothermal resource. The total heat flow through the experimental site surface has been measured, with a high average of 536 W/m^2 and an uneven distribution along the site surface. The overall heat flow data generally follows a normal-like distribution characterized by the following statistical quantities: $q\sim N$ (649, 714^2). And based on the finite element method, the mean waste heat flow through the whole fire zone is computed to be 495 W/m^2, while an average utilization rate of 58%.

A thermodynamic model of WHRUS has been proposed to quantify the heat extraction, on which is based to derive the sub-thermal resistances (W/°C) of HP, heat source and cooling source, turning out to be 0.0048988, 0.0021732 and 0.00195511 respectively. WHRUS was comprehensively tested and performed with exceptional isothermality and stability. Meanwhile, the thermal balance was analyzed to be aware of the existence of heat nonequilibrium (5.5%) due to the heat loss and inherent defects of equipment.

Furthermore, the average waste heat output is theoretically deduced to be 46 kW per hole, 94% of which can be recovered by WHRUS. Waste heat in the fire zone was well utilized as direct heating and indirect thermoelectric conversion. A temperature difference around 50 °C can produce the maximum power of 1587 W for a single hole, and the output has been stable delivering an average above 960 W per month. The conversion efficiency of Be_2Te_3 based material is low. However, taking advantages of the huge capacity, low expense and easy of availability, the waste heat of underground coal fires can certainly meet the demand of practical power generation in commercial terms. The rest of heat egress is mainly absorbed by water (93%)

that can be used for the heating of the local district. This heating enables to maintain indoor temperatures above 20 °C at a measured heating efficiency of 38%.

Finally, the potential benefits delivered by the whole fire zone are remarkable in terms of resource, energy-saving and economy. There is total 105.199 MW/a waste heat estimated to be recoverable from the whole fire field, which can be potentially reusable for electricity generation (10^6 kWh/a) and district heating (1.331×10^5 m^2/a), while saving a large amount of water (4.55×10^5/a) for fire suppression.

Acknowledgments

This research was funded by 111 Project (Grant No. B17041), National Natural Science Foundation of China (Grant No. 51704283), and Natural Science Foundation of Jiangsu Province (Grant No. BK20170277).

Reference

[1] Lang L, Zhou FB. A comprehensive hazard evaluation system for spontaneous combustion of coal in underground mining. International Journal of Coal Geology 2010;82:27-36.

[2] Zhang JM. Research and control of underground coal fire in China. Beijing: Coal Industry Press; 2008.

[3] Song Z, Kuenzer C. Coal fires in China over the last decade: A comprehensive review. International Journal of Coal Geology 2014;133:72-99.

[4] Li Z, Kong B, Wei A, et al. Free radical reaction characteristics of coal low-temperature oxidation and its inhibition method. Environmental Science and Pollution Research 2016;23:23593-23605.

[5] Kong B, Li Z, Yang Y, et al. A review on the mechanism, risk evaluation, and prevention of coal spontaneous combustion in China. Environmental Science and Pollution Research 2017;24: 23453-23470.

[6] Zhang Y, Hu S R, Yue T, et al. Environmental Effect Analysis of Coalfield Fire in Xinjiang and its Preventive. Advanced Materials Research 2014;1010-1012:601-605.

[7] Kuenzer C, Stracher G B. Geomorphology of coal seam fires. Geomorphology 2012;138:209-222.

[8] Wu JJ, Liu XC. Risk assessment of underground coal fire development at regional scale. International Journal of Coal Geology 2011;86:87-94.

[9] Stracher G B, Taylor T P. Coal fires burning out of control around the world: thermodynamic recipe for environmental catastrophe. International Journal of Coal Geology 2004;59:7-17.

[10] Finkelman R B. Potential health impacts of burning coal beds and waste banks. International Journal of Coal Geology 2004;59:19-24.

[11] Kuenzer C, Zhang J, Tetzlaff A, et al. Uncontrolled coal fires and their environmental impacts: Investigating two arid mining regions in north-central China. Applied Geography 2007;27:42-62.

[12] Querol X, Zhuang X, Font O, et al. Influence of soil cover on reducing the environmental impact of spontaneous coal combustion in coal waste gobs: A review and new experimental data. International Journal of Coal Geology 2011;85:2-22.

[13] Zhao Y, Zhang J, Chou CL, et al. Trace element emissions from spontaneous combustion of gob piles in coal mines,

Shanxi, China. International Journal of Coal Geology 2008;73:52-62.

[14] Wu JJ, Jiang WG, Liu XC, et al. Innovative technologies for exploration, monitoring and extinction of underground coal fires. Journal of China Coal Society 2009;34:1669-1674.

[15] Wu JM, Zhang JH, Wu YG. detection on Spontaneous Combustion Area in Surface Mine and Study on Comprehensive Control Technology of Spontaneous Combustion Area. Coal Engineering 2012;(2):53-56

[16] Shao ZL, Jia XY, Zhong XX, et al. Detection, extinguishing, and monitoring of a coal fire in Xinjiang, China. Environmental Science and Pollution Research 2018;25:26603-26616.

[17] Shi B, Su H, Li J, et al. Clean power generation from the intractable natural coalfield fires: turn harm into benefit. Scientific Reports 2017;7:5302.

[18] Wessling S, Kuenzer C, Kessels W, et al. Numerical modeling for analyzing thermal surface anomalies induced by underground coal fires. International Journal of Coal Geology 2008;74:175-184.

[19] Aswal D K, Basu R, Singh A. Key issues in development of thermoelectric power generators: High figure-of-merit materials and their highly conducting interfaces with metallic interconnects. Energy Conversion and Management 2016;114:50-67.

[20] Shao Z, Wang D, Wang Y, et al. Controlling coal fires using the three phase foam and water mist techniques in the Anjialing Open Pit Mine, China. Natural Hazards 2015;75:1833-1852.

[21] Chaudhry H N, Hughes B R, Ghani S A. A review of heat pipe systems for heat recovery and renewable energy applications. Renewable and Sustainable Energy Reviews 2012;16:2249-2259.

[22] Jouhara H, Chauhan A, Nannou T, et al. Heat pipe based systems - Advances and applications. Energy 2017;128:729-754.

[23] Zohuri, Bahman. Heat Pipe Design and Technology. Germany: Springer. 2016.

[24] Saeed Tiari, Mahboobe Mahdavi, Songgang Qiu. Experimental study of a latent heat thermal energy storage system assisted by a heat pipe network. Energy Conversion and Management 2017;153:362-373.

[25] Franco A, Vaccaro M. On the use of heat pipe principle for the exploitation of medium–low temperature geothermal resources. Applied Thermal Engineering 2013;59:189–199.

[26] Jang JC, Chi RG, Rhi HS. Heat Pipe-Assisted Thermoelectric Power Generation Technology for Waste Heat Recovery. Journal of Electronic Materials 2015;44:2039-2047.

[27] Abdellah Shafieian, Mehdi Khiadani, Ataollah Nosrati. Strategies to improve the thermal performance of heat pipe solar collectors in solar systems: A review. Energy Conversion and Management 2019;183:307-331

[28] Schmidt M, Suhendra, Rueter H. Coal Fire Fighting: Removal of Thermal Energy by Heat Pipes. EGU General Assembly 2009, p. 12440.

[29] Li B, Deng J, Xiao Y, et al. Heat transfer capacity of heat pipes: An application in coalfield wildfire in China. Heat and Mass Transfer 2018;54:1755-1766.

[30] Zhang Y, Zhao L, Fan Z, et al. Temperature distribution of fluids in a two-section two-phase closed thermosyphon wellbore. Petroleum Science 2014;11:287-292.

[31] Díez, Rafael, Díaz-Aguado, María. Estimating Limits for the Geothermal Energy Potential of Abandoned Underground Coal Mines: A Simple Methodology. Energies 2014;7:4241-4260.

[32] Peralta R E, Breede K, Falcone G. Geothermal heat recovery from abandoned mines: a systematic review of projects implemented worldwide and a methodology for screening new projects. Environmental Earth Sciences 2015;73:6783-6795.

[33] Liu YJ. Waste Heat Utility Technology in Coal Mine. Applied Mechanics and Materials 2012;170-173:2723-2726.

[34] Kajikawa T. Approach to the Practical Use of Thermoelectric Power Generation. Journal of Electronic Materials 2009;38:1083-1088.

[35] Zheng XF, Boukhanouf R. Experimental study of a domestic thermoelectric cogeneration system. Applied Thermal Engineering 2014;62:69-79.

[36] Karri M A, Thacher E F, Helenbrook B T. Exhaust energy conversion by thermoelectric generator: Two case studies. Energy Conversion and Management 2011;52:1596-1611.

[37] Tundee S, Srihajong N, Charmongkolpradit S. Electric Power Generation from Solar Pond Using Combination of Thermosyphon and Thermoelectric Modules. Energy Procedia 2014;48:453-463.

[38] Daniel Champier. Thermoelectric generators: A review of applications. Energy Conversion and Management 2017;140:167-181.

[39] Leyre Catalan, Patricia Aranguren, Miguel Araiz, Gurutze Perez, David Astrain. New opportunities for electricity generation in shallow hot dry rock fields: A study of thermoelectric generators with different heat exchangers. Energy Conversion and Management 2019;200:112061.

[40] Zheng XF, Liu CX, Yan YY, et al. A review of thermoelectrics research-Recent developments and potentials for sustainable and renewable energy applications. Renewable and Sustainable Energy Reviews 2014;32:486-503.

[41] He W, Zhang G, Zhang X, et al. Recent development and application of thermoelectric generator and cooler. Applied Energy 2015;143:1-25.

[42] Champier, Daniel. Thermoelectric generators: A review of applications. Energy Conversion and Management 2017;140:167-181.

[43] Liu W, Jie Q, Kim H S, et al. Current progress and future challenges in thermoelectric power generation: From materials to devices. Acta Materialia 2015;87:357-376.

[44] Su H, Zhou F, Qi H, et al. Design for Thermoelectric Power Generation Using Subsurface Coal Fires. Energy 2017;140:929-940.

[45] Su HT, Qi HN, Liu P, et al. Experimental investigation on heat extraction using a two-phase closed thermosyphon for thermoelectric power generation. Energy Sources, Part A: Recovery, Utilization, and Environmental Effects 2018;40:1485-1490.

[46] GOLDEN SOFTWARE. Sufer® - version 8.03. Golden, 2003. Software. http://www.goldensoftware.com/ demo.shtml. 13 jan. 2006.

[47] Trefethen L N. Spectral methods in MATLAB. SIAM. 2000.

[48] Imura H, Sasaguchi K, Kozai H, et al. Critical heat flux in a closed two-phase thermosyphon. International Journal of Heat and Mass Transfer 1983;26:1181-1188.

[49] D.A. Reay, P.A. Kew, R.J. McGlen. Heat Pipes (Theory, Design and Applications). 6th ed. In: Chapter 2-Heat transfer and fluid flow theory, London: Elsevier Science Ltd;2014, p. 15-64.

[50] Jafari D, Franco A, Filippeschi S, et al. Two-phase closed thermosyphons: A review of studies and solar applications. Renewable and Sustainable Energy Reviews 2016;53:575-593.

[51] Rohsenow WM, Hartnett JP, Ganic EN. Handbook of heat transfer fundamentals (2nd edition). Journal of Applied Mechanics 1986;53:232-233.

[52] Hamidreza S, Michael JA, Nourouddin S, et al. Heat pipe heat exchangers and heat sinks: Opportunities, challenges, applications, analysis, and state of the art. International Journal of Heat and Mass Transfer 2015;89:138-158.

[53] Zhang X, Zhao LD. Thermoelectric materials: Energy conversion between heat and electricity. Journal of Materiomics 2015;1:92-105.

[54] Yang JH. Special section papers on thermoelectric materials and applications-foreword. J Electron Mater 2007;36:703.

[55] Yu S, Du Q, Diao H, et al. Effect of vehicle driving conditions on the performance of thermoelectric generator. Energy Conversion and Management 2015;96:363-376.

[56] Dai KY. Preliminary report of the fire extinguishing project in the fire field of Sandaoba Coalfield, Miquan. Xinjiang: Coal Industry Xian Design & Research Institute; 2017.